the cell death seen with the P23H rhodopsin mutation. Similarly, insufficient or imbalanced UPR output could also trigger cell loss in other diseases that arise from persistent ER stress.

### References and Notes


1. D. Ron, P. Walter, *Nat. Rev. Mol. Cell Biol.* **8**, 519 (2007).
2. M. Calfon *et al.*, *Nature* **415**, 92 (2002).
3. H. Yoshida, T. Matsui, A. Yamamoto, T. Okada, K. Mori, *Cell* **107**, 881 (2001).
4. A. H. Lee, N. N. Iwakoshi, L. H. Glimcher, *Mol. Cell. Biol.* **23**, 7448 (2003).
5. H. P. Harding, Y. Zhang, D. Ron, *Nature* **397**, 271 (1999).
6. H. P. Harding *et al.*, *Mol. Cell* **6**, 1099 (2000).
7. K. Haze, H. Yoshida, H. Yanagi, T. Yura, K. Mori, *Mol. Biol. Cell* **10**, 3787 (1999).
8. J. Ye *et al.*, *Mol. Cell* **6**, 1355 (2000).
9. J. A. Morris, A. J. Dorner, C. A. Edwards, L. M. Hendershot, R. J. Kaufman, *J. Biol. Chem.* **272**, 4327 (1997).
10. H. Zinszner *et al.*, *Genes Dev.* **12**, 982 (1998).
11. J. L. Garrison, E. J. Kunkel, R. S. Hegde, J. Taunton, *Nature* **436**, 285 (2005).
12. F. Urano *et al.*, *Science* **287**, 664 (2000).
13. J. Shen, R. Prywes, *Methods* **35**, 382 (2005).
14. F. R. Papa, C. Zhang, K. Shokat, P. Walter, *Science* **302**, 1533 (2003).
15. W. Tirasophon, K. Lee, B. Callaghan, A. Welihinda, R. J. Kaufman, *Genes Dev.* **14**, 2725 (2000).
16. X. Z. Wang *et al.*, *EMBO J.* **17**, 5708 (1998).
17. H. R. Cohen, B. Panning, *Chromosoma* **116**, 373 (2007).
18. M. Schroder, R. J. Kaufman, *Annu. Rev. Biochem.* **74**, 739 (2005).
19. M. M. Sohocki *et al.*, *Hum. Mutat.* **17**, 42 (2001).
20. C. H. Sung, C. M. Davenport, J. Nathans, *J. Biol. Chem.* **268**, 26645 (1993).
21. S. Kaushal, H. G. Khorana, *Biochemistry* **33**, 6121 (1994).
22. H. F. Mendes, J. van der Spuy, J. P. Chapple, M. E. Cheetham, *Trends Mol. Med.* **11**, 177 (2005).
23. R. H. Steinberg *et al.*, *Invest. Ophthalmol. Visual Sci.* **37**, Association for Research in Vision and Ophthalmology (ARVO) Abstract 3190, S698 (1996).
24. S. Machida *et al.*, *Invest. Ophthalmol. Visual Sci.* **41**, 3200 (2000).
25. D. T. Rutkowski *et al.*, *PLoS Biol.* **4**, 374 (2006).
26. D. Acosta-Alvear *et al.*, *Mol. Cell* **27**, 53 (2007).
27. S. H. Back, M. Schroder, K. Lee, K. Zhang, R. J. Kaufman, *Methods* **35**, 395 (2005).
28. Single-letter abbreviations for the amino acid residues are as follows: A, Ala; C, Cys; D, Asp; E, Glu; F, Phe; G, Gly; H, His; I, Ile; K, Lys; L, Leu; M, Met; N, Asn; P, Pro; Q, Gln; R, Arg; S, Ser; T, Thr; V, Val; W, Trp; and Y, Tyr.


29. We thank the Walter lab, B. Farese, J. L. Garrison, R. J. Kaufman, R. Locksley, M. Matthes, D. Morgan, J. Nathans, R. Prywes, F. Sanchez, and B. Yen for comments, provision of reagents, or technical advice. This work was supported by the Amyotrophic Lateral Sclerosis Association, U.S. Department of Defense, Foundation Fighting Blindness, John Douglas French Alzheimer's Foundation, National Eye Institute, NIH, and Research to Prevent Blindness. P.W. and K.M.S. are Howard Hughes Medical Institute Investigators.


### Supporting Online Material

www.sciencemag.org/cgi/content/full/318/5852/944/DC1
Materials and Methods
Figs. S1 to S3
References


12 June 2007; accepted 7 September 2007
10.1126/science.1146361




# The Simplest Double Slit: Interference and Entanglement in Double Photoionization of $H_2$


**D. Akoury,[1,2] K. Kreidi,[1] T. Jahnke,[1] Th. Weber,[1,2] A. Staudte,[1] M. Schöffler,[1] N. Neumann,[1] J. Titze,[1] L. Ph. H. Schmidt,[1] A. Czasch,[1] O. Jagutzki,[1] R. A. Costa Fraga,[1] R. E. Grisenti,[1] R. Díez Muiño,[3] N. A. Cherepkov,[4] S. K. Semenov,[4] P. Ranitovic,[5] C. L. Cocke,[5] T. Osipov,[2] H. Adaniya,[2] J. C. Thompson,[6] M. H. Prior,[2] A. Belkacem,[2] A. L. Landers,[6] H. Schmidt-Böcking,[1] R. Dörner[1]***



**The wave nature of particles is rarely observed, in part because of their very short de Broglie wavelengths in most situations. However, even with wavelengths close to the size of their surroundings, the particles couple to their environment (for example, by gravity, Coulomb interaction, or thermal radiation). These couplings shift the wave phases, often in an uncontrolled way, and the resulting decoherence, or loss of phase integrity, is thought to be a main cause of the transition from quantum to classical behavior. How much interaction is needed to induce this transition? Here we show that a photoelectron and two protons form a minimum particle/slit system and that a single additional electron constitutes a minimum environment. Interference fringes observed in the angular distribution of a single electron are lost through its Coulomb interaction with a second electron, though the correlated momenta of the entangled electron pair continue to exhibit quantum interference.**


One of the most powerful paradigms in the exploration of quantum mechanics is the double-slit experiment. Thomas Young was the first to perform such an experiment, as early as 1801, with light. It took until the late 1950s (*1*), long after the experimental proof of the wave nature of particles was revealed, for a similar experiment to be carried out with electrons. Today, such experiments have been demonstrated for particles as heavy as $C_{60}$ (*2*) and for bound electrons inside a highly excited atom (*3*). All of these experiments were aimed at a demonstration of double-slit self interference for a single particle fully isolated from the environment. If, however, this ideal laboratory situation is relaxed and the quantum particles are put in contact with the environment in a controlled manner, the quantum interference may be diminished so that the particles start behaving in an increasingly classical way (*4*–*6*). Recently, Hackermüller *et al.* (*7*) have demonstrated this phenomenon by sending heated $C_{60}$ clusters through a double slit. The hot molecules couple via the emission of thermal photons to the environment, and a loss of interference as a function of their temperature is observed. The emission of the photons alters the relative phase between different pathways of the particle toward the detector, an effect referred to as decoherence. Such decoherence of a quantum system can be caused by single or multiple interactions with an external system (*6*). Limiting cases are one single hard interaction causing the decoherence by entanglement with the external system and multiple weak couplings to external perturbers (for instance, a bath) at the other extreme. A gradual transition between these two extremes has been demonstrated for photon scattering (*6*).

We experimentally demonstrated that a system of two electrons is already sufficient to observe the transition from a quantum interference pattern to a classical particle-like intensity distribution for an individual electron. The quantum coherence is not destroyed, however, but remains in the entangled two-electron system. By measuring the correlated momenta of both particles, we illustrate this interference pattern, which is otherwise concealed in the two-body wave function.

The idea of using a homonuclear molecule as the slit-scattering center of a photoelectron goes back to a paper published in 1966 by Cohen and Fano (*8*). Because of the coherence in the initial molecular state, the absorption of one


[1]Institut für Kernphysik, University Frankfurt, Max von Laue Str 1, D-60438 Frankfurt, Germany. [2]Lawrence Berkeley National Laboratory, Berkeley, CA 94720, USA. [3]Centro de Física de Materiales and Donostia International Physics Center, 20018 San Sebastián, Spain. [4]State University of Aerospace Instrumentation, 190000 St. Petersburg, Russia. [5]Department of Physics, Kansas State University, Cardwell Hall, Manhattan, KS 66506, USA. [6]Department of Physics, Auburn University, Auburn, AL 36849, USA.

*To whom correspondence should be addressed. E-mail: doerner@atom.uni-frankfurt.de

photon by the homonuclear molecule launches two coherent electron waves at each of the protons of the molecule (Fig. 1, A and B). The interference pattern of these waves should be visible in the angular distribution of the electron, with respect to the molecular axis. In K shell ionization of heavy diatomics (e.g., $N_2$ and $O_2$, as discussed by Cohen and Fano), interference is visible only if the symmetry (gerade or ungerade) of the molecule with a single 1s hole is resolved (*9*, *10*). For ground-state $H_2^+$ and $H_2$ molecules, only gerade orbitals are populated, and thus these systems constitute clean cases where slitlike behavior is expected (*11*). Still, the originally proposed experiment on $H_2$ (*11*) has not been carried out, because it requires knowledge of the direction of the molecular axis (*12*, *13*). A signature of the interference effect has nonetheless been observed in the wavelength dependence of electrons emitted from a randomly oriented sample of $H_2$ molecules by ion impact ionization (*14*, *15*).

We extended the idea of Cohen and Fano from single photoionization to double photoionization to study the two-body interference of an electron pair. This electron pair is emitted by absorption of a single circularly polarized photon from the $H_2$ molecule (Eq. 1)

$$h\nu + H_2 \rightarrow 2p^+ + 2e^- \qquad (1)$$

$h\nu$ symbolizes a photon of frequency ν. The two electrons are distinguishable by their energy, which allows us to study the interference pattern as a function of the interaction strength or momentum exchanged between the two particles.

Single photons from beamlines 4.0 or 11.0 at the Advanced Light Source at Lawrence Berkeley National Laboratory were used to photoeject both electrons of each $H_2$ molecule. A supersonic $H_2$ gas jet was crossed with the photon beam. For each ionized molecule, the vector momenta of all fragment particles—both ions and both electrons—were determined in coincidence. The orientation of the $H_2$ molecule, or molecular double slit, was measured for each fragmentation by detecting the emission direction of the two protons. Once the two electrons are ejected, the protons rapidly fly apart along the molecular axis, driven by their mutual Coulomb repulsion. A multiparticle imaging technique (cold target recoil ion momentum spectroscopy) (*16*, *17*) was used to detect all particles. The ions and electrons created in the intersection volume of the photon and gas beams were guided by weak electric (50 V/cm) and magnetic fields (8 G) toward two separate multichannel plate detectors with delayline readouts (*18*). From the position of impact and the time of flight, the initial vector momentum of each particle can be determined. Only three particles (two protons and one electron) need to be detected. The momentum of the second electron (in the present case the more energetic of the two) is deduced through momentum conservation of the total system. The Coulomb explosion of the two protons at the equilibrium distance of $H_2$ of 1.4 atomic units (au) yields a kinetic energy of about 10 eV per proton (*19*), and the total electronic binding energy of $H_2$ is about 30 eV. The experiment has been performed at two different photon energies of $E_\gamma = 240$ and 160 eV, leaving about 190 and 110 eV of energy to be shared among the two electrons, respectively. At the high photon energies under consideration here, double photoionization of $H_2$ leads in most cases to one fast electron and one slow electron (*20*).

Figure 1D shows, for ionization by 240-eV photons, the measured angular distribution for a highly energetic electron (called "1" here) of energy $E_1$: 185 eV < $E_1$ < 190 eV. The second electron, unobserved here, acquires an energy of only $E_2$ < 5 eV. The angular distribution is in the plane perpendicular to the photon propagation vector, and the molecular axis is oriented horizontally in that plane. (The data plotted include events where electron 1 and the molecular axis lie within 10 degrees of the ideal plane perpendicular to the photon propagation direction)

The experimental data show a strong interference pattern that qualitatively resembles the pattern induced by a double slit. For the optical double-slit experiment in which the interference results from a superposition of two coherent spherical waves, the intensity distribution I is given by Eq. 2

$$I(\Phi_{e-mol}) = C\cos^2\left[\frac{k_e \times R \times \cos(\Phi_{e-mol})}{2}\right] \qquad (2)$$

In our case, $R$ is the internuclear distance (1.4 au for $H_2$), $\Phi_{e-mol}$ is the angle of electron emission with respect to the internuclear axis (*12*), $k_e$ is the momentum of the electron, and $C$ is a proportionality constant. An electron energy of 190 eV (as in Fig. 1) corresponds to $k_e = 3.75$ au. The double-slit prediction of Eq. 2 is shown by the blue line in Fig. 1E.

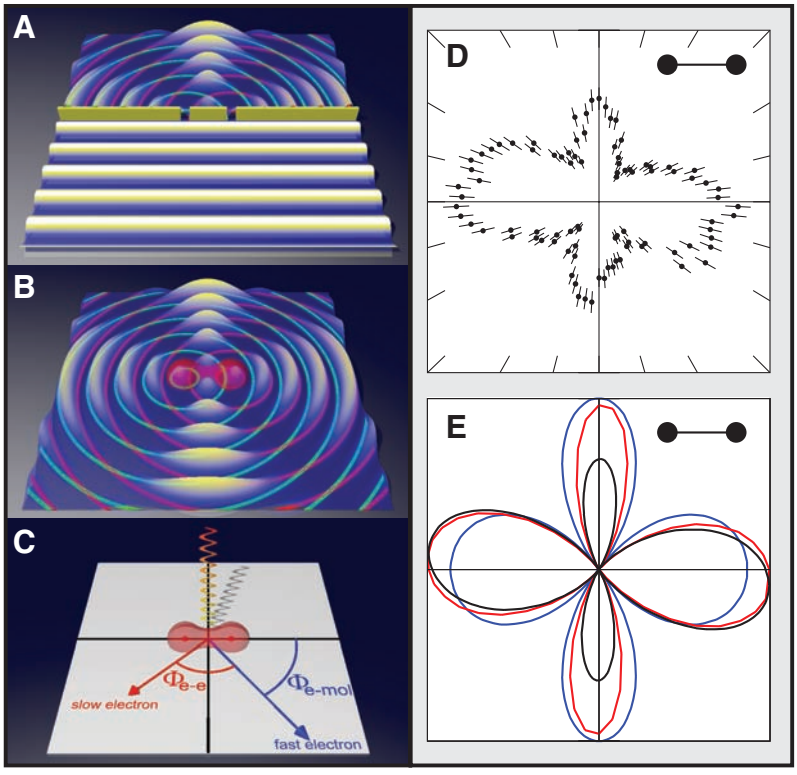


**Fig. 1.** (**A**) Schematic view of a double-slit arrangement. A plane wave approaches the slit from the front. The slit separation is 1.4 au (the internuclear distance in $H_2$), and the wavelength is 3.75 au, which corresponds to an electron energy of 190 eV. (**B**) Photoionization by circularly polarized light launches a coherent spherical photoelectron wave at each nucleus of the molecule; the light propagates into the plane. (**C**) Geometry of the present experiment; circularly polarized light comes from the top. All angular distributions shown in this paper are in the plane perpendicular to the photon propagation vector, $\Phi_{e-mol}$ is the angle of the fast electron's trajectory to the molecular axis, and $\Phi_{e-e}$ is the angle between both electron trajectories. (**D**) Measured electron angular distribution ($\Phi_{e-mol}$) of the faster electron from double photoionization of $H_2$ by circularly polarized light. The orientation of the molecule is horizontal. Light propagates into the plane of the figure, the molecule is fixed ±10° within the plane shown, $E_\gamma = 240$ eV, and the energy of the slow electron $E_2 = 0$ to 5 eV, resulting in $E_1 = 185$ to 190 eV. (**E**) Angular probability distributions derived from Eq. 2 (blue line), RPA calculation (red), and multiple scattering calculation (black).

The deviations from the double-slit prediction can be understood from the somewhat more elaborate theoretical treatment shown in Fig. 1E. By treating the electrons as spherical waves, the simple approximation in Eq. 2 neglects the fact that the electrons are ejected by circularly polarized light and further that they must escape from the two-center Coulomb potential of the two nuclei. The helicity of the light leads to a slight clockwise rotation of the angular distribution, as seen in the experiment and the more elaborate calculations. The Coulomb interaction with the nuclei has two major effects. First, the wavelength of the electron in the vicinity of the protons is shorter than the asymptotic value. This property modifies, in particular, the emission probability along the molecular axis due to a phase shift in the nearfield (*21*). Second, the original partial wave emerging from one of the nuclei is scattered at the neighboring nucleus, thereby launching another partial wave. Thus, the final diffraction pattern is the superposition of four (or more) coherent contributions: the primary waves from the left and right nuclei and the singly or multiply scattered waves created subsequently in the molecular potential. We performed two calculations to take the helicity of the photon, as well as multiple scattering effects, into account. The first calculation (red line in Fig. 1E) was based on the random phase approximation (RPA) (*22*), and the second (black line in Fig. 1E) entailed a multiple scattering calculation, wherein a spherical wave is launched at one proton (*23*). This wave is then multiply scattered in the two-center potential of two protons, which is terminated at a boundary. The direct and multiple scattered waves are then coherently added and symmetrized. Although conceptually very different, both calculations account for all of the relevant physical features: the two-center interference determining the position of minima and maxima, the molecular potential altering the relative height of the peaks, and the helicity of the ionizing photon inducing a rotation. The details of the molecular potential differ in the calculations. The RPA uses a Hartree-Fock potential, whereas the multiple scattering calculation assumes two bare protons.

The full calculations treat the emission of a single electron. Therefore, their good agreement with the experimental data (Fig. 1D) obtained from double ionization might be surprising. This suggests that the additional emission of a slow electron does not substantially alter the wave of the fast particle. For the particular case in which the electron pair consists of a fast and a very slow electron, the diffraction of a coherent electron pair can be treated by simply neglecting the slow electron.

This simple one-particle picture completely fails in scenarios where lower primary and higher scattered electron energies result in stronger coupling between the electrons. Figure 2, A and B, shows the results for different energy partitions of the first and second electron after ionization by 160-eV photons. Whereas for $E_1 \approx 110$ eV and $E_2 < 1$ eV the interference is still visible (Fig. 2A), it completely disappears when $E_1 \approx 95$ eV and 5 eV $< E_2 <$ 25 eV (Fig. 2B). In the latter case, the distribution approaches the isotropic result without two-center interference. By comparing these data to the corresponding theoretical estimates (Fig. 2, C and D), we can now show that the observed loss of interference contrast is a result of decoherence and not of the changing electron wavelength.

Coulomb interaction between two quantum mechanical systems (electrons 1 and 2 in our case) does not destroy phases. Rather, it entangles the wave functions of the two subsystems (*24*, *5*). In our experiment, we observed both electrons in coincidence. Therefore we can investigate this entangled two-particle system to search for the origin of the apparent loss of coherence in a single-particle subsystem. Figure 3 shows the correlation in this two-body system. The horizontal axis is the angle of the fast-electron momentum, with respect to the molecular axis (i.e., the angle that is plotted in all other figures). The vertical axis is the angle between the two electron's momenta. It may be helpful to think of the horizontal axis as the scattering of electron 1 by the double slit and the vertical axis as the scattering angle between the electrons. Marked interference patterns emerge in this display of the two-particle wave function. No vestige of these patterns remains, however, if the distribution is integrated over the vertical axis.

When subsets of the data with restricted angular ranges of $\Phi_{e-e} = +70 \pm 20°$ (Fig. 3, B and C) and $\Phi_{e-e} = -70 \pm 20°$ (Fig. 3, D and E) are examined, then the interference pattern is resurrected (here, $\Phi_{e-e}$ is the angle between both electron trajectories). However, depending on the angle between the electrons in the selected subset of the data, the interference pattern is tilted to the right (Fig. 3C) or left (Fig. 3E). Without the restriction of this relative angle, the shifted minima and maxima cancel each other out, leading to the almost isotropic distribution of Fig. 2B.

The interference maxima are concentrated along two horizontal lines. These lines of highest intensity lie at a relative angle of about 100° between the two electrons. This distribution is a well-known indication of the mechanism whereby the absorption of a single photon by one electron can induce its ejection, as well as that of the other electron, after their binary collision

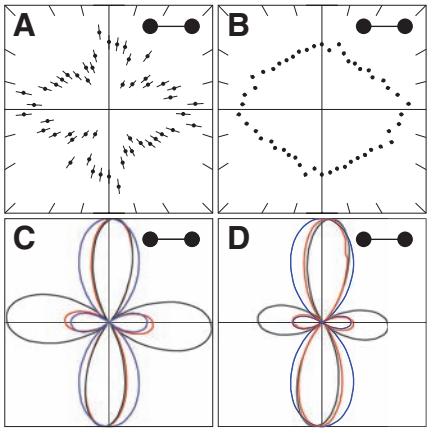


**Fig. 2.** (**A**) Electron angular distribution as in Fig. 1D but for $E_\gamma = 160$ eV, $E_2 < 1$ eV, and $E_1 \approx 110$ eV. (**B**) $E_\gamma = 160$ eV and 5 eV $< E_2 <$ 25 eV, resulting in $E_1 \approx 85$ to 105 eV. (**C** and **D**) Angular distribution of a single electron of energy $E_e$ for the energy distributions in (A) and (B), respectively. Red, Eq. 2; blue, RPA calculation; black, multiple scattering calculation.

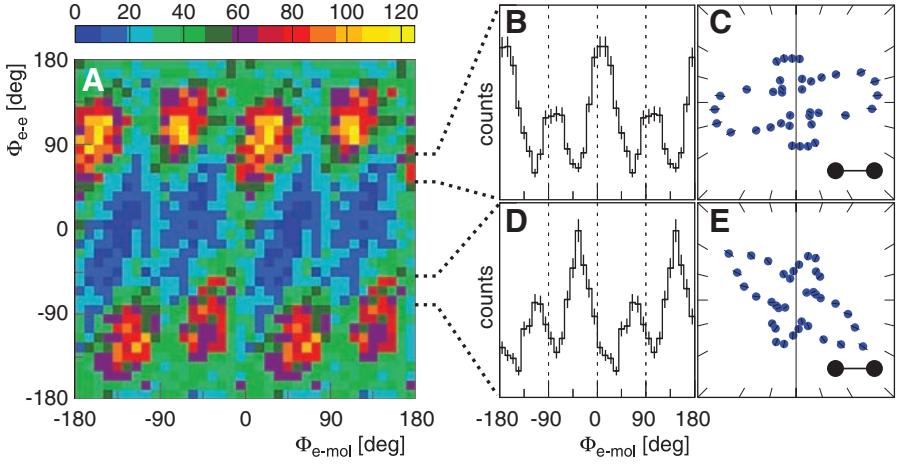


**Fig. 3.** Correlation between both electrons for double photoionization of $H_2$ at $E_\gamma = 160$ eV and 5 eV $< E_2 <$ 25 eV, corresponding to $E_1 \approx 85$ to 105 eV. (**A**) *x* axis: angle of fast electron to the molecular axis ($\Phi_{e-mol}$) (see Fig. 1C), and *y* axis: angle $\Phi_{e-e}$ between the two electrons. Both electrons and the molecule are selected to lie within ±30° of the polarization plane. Thus, Fig. 2B is a projection of this figure onto the horizontal axis. (**B**) Projection of (A) onto the horizontal axis for 50° $< \Phi_{e-e} <$ 80°. (**C**) Polar presentation of the data shown in (B). (**D**) Projection analogous to (B) for −80° $< \Phi_{e-e} <$ −50°. (**E**) Polar presentation of data shown in (D).

(*20*, *25*). The angles $\Phi_{e-e} = 90°$ and $\Phi_{e-e} = -90°$ correspond to a kick of the second electron, either to the left or the right. This strong electron-electron Coulomb interaction mediates the double ionization and creates an entanglement between the two electrons. Electron collisions of this sort in bound systems have been demonstrated directly in pump-probe experiments (*26*).

This situation is an intramolecular version of a scattering event downstream of a double slit (*27*, *6*). When either photons (*6*) or particles (*27*) are scattered from a beam after passage through a double slit, the scattering induces a phase shift, which then leads to a shift of the interference pattern. If the momentum transfer is not measured in coincidence (*6*), the fringe visibility is lost. In this experiment, both electrons are initially delocalized inside the molecule in a completely coherent single quantum state. Before photoabsorption, both electrons are confined in the hydrogen ground state, which is symmetric with respect to its two atomic centers. Thus, we observed not a scattering between classical localized particles but a coherent entanglement of the wave function of the two electrons.

It is instructive to think of the electronic two-body system as split into its subsystems and to consider one subsystem as the environment of the other. The strong Coulomb interaction entangles the two subsystems and leads to a position-dependent modification of phase of the single-particle wave function inside each of the two subsystems. The entanglement of the electrons in the pair is directly visible in their mutual angular distribution and is further evidenced by the observation that selecting the momentum of one electron makes the interference pattern of its partner reappear. In the spirit of discussions dating from the early history of quantum mechanics, one particle can be considered an observer that carries partial information about the other particle and its path through the double slit. The amount of which-way information exchanged between the particles is limited by the observer particle's de Broglie wavelength (*28*). The key difference between the situation depicted in Fig. 2A (which shows interference) and Fig. 2B (which shows no interference) is that the wavelength of the second, unobserved electron is much shorter in the latter case.

Our experiment thus reveals that a very small number of particles suffices to induce the emergence of classical properties, such as the loss of coherence. A four-body system, such as fragmented molecular hydrogen, acts as a double slit in the sense that coherence is lost in a subsystem of entangled electrons. Such a fundamental system facilitates the study of the influence of interelectronic Coulomb interactions on the coherence properties of a single electron. In solid-state–based quantum computing devices, such electron-electron interaction represents a key challenge. One advantageous aspect of the finite system investigated here is that, theoretically, it is fully tractable at present (*29*–*32*).

### References and Notes


1. C. Jönnson, *Z. Phys. A* **161**, 454 (1961).
2. M. Arndt *et al.*, *Nature* **401**, 680 (1999).
3. M. Noel, C. Stroud, *Phys. Rev. Lett.* **75**, 1252 (1995).
4. E. Joos, H. Zeh, *Z. Phys. B* **59**, 223 (1985).
5. W. Zurek, *Rev. Mod. Phys.* **75**, 715 (2003).
6. D. A. Kokorowski, A. D. Cronin, T. D. Roberts, D. E. Pritchard, *Phys. Rev. Lett.* **86**, 2191 (2001).
7. L. Hackermüller, K. Hornberger, B. Brezger, A. Zeilinger, M. Arndt, *Nature* **427**, 711 (2004).
8. H. Cohen, U. Fano, *Phys. Rev.* **150**, 30 (1966).
9. D. Rolles *et al.*, *Nature* **7059**, 711 (2005).
10. X. Liu *et al.*, *J. Phys. B* **39**, 4801 (2006).
11. I. Kaplan, A. Markin, *Sov. Phys. Dokl.* **14**, 36 (1969).
12. M. Walter, J. Briggs, *J. Phys. B* **32**, 2487 (1999).
13. J. Fernandez, O. Fojon, A. Palacios, F. Martín, *Phys. Rev. Lett.* **98**, 043005 (2007).
14. N. Stolterfoht *et al.*, *Phys. Rev. Lett.* **87**, 023201 (2001).
15. D. Misra *et al.*, *Phys. Rev. Lett.* **92**, 153201 (2004).
16. J. Ullrich *et al.*, *Rep. Prog. Phys.* **66**, 1463 (2003).
17. R. Dörner *et al.*, *Phys. Rep.* **330**, 95 (2000).
18. O. Jagutzki *et al.*, *Nucl. Instrum. Methods A* **477**, 244 (2002).
19. T. Weber *et al.*, *Nature* **431**, 437 (2004).
20. A. Knapp *et al.*, *Phys. Rev. Lett.* **89**, 033004 (2002).
21. G. L. Yudin, S. Chelkowski, A. D. Bandrauk, *J. Phys. B* **39**, L17 (2006).
22. S. K. Semenov, N. A. Cherepkov, *J. Phys. B* **36**, 1409 (2003).
23. R. Díez Muiño, D. Rolles, F. J. García de Abajo, C. S. Fadley, M. A. Van Hove, *J. Phys. B* **35**, L359 (2002).
24. T. Opatrny, G. Kurizki, *Phys. Rev. Lett.* **86**, 3180 (2001).
25. M. Pont, R. Shakeshaft, *Phys. Rev. A* **51**, R2676 (1995).
26. S. N. Pisharody, R. R. Jones, *Science* **303**, 813 (2004).
27. K. Hornberger *et al.*, *Phys. Rev. Lett.* **90**, 160401 (2003).
28. W. Wootters, W. Zurek, *Phys. Rev. D* **19**, 473 (1979).
29. W. Vanroose, F. Martín, T. Rescigno, C. W. McCurdy, *Science* **310**, 1787 (2005).
30. F. Martín *et al.*, *Science* **315**, 629 (2007).
31. J. Colgan, M. S. Pindzola, F. Robicheaux, *J. Phys. B* **37**, L377 (2004).
32. D. Dundas, *J. Phys. B* **37**, 2883 (2004).



33. We thank M. Walter, J. Briggs, A. Kheifets, U. Becker, D. Rolles, E. Joos, K. Ueda, M. Arndt, and M. Aspelmeyer for enlightening discussions. We acknowledge outstanding support by the staff of the Advanced Light Source, in particular by E. Arenholz, T. Young, H. Bluhm, and T. Tyliszczak. This work was supported by the Deutsche Forschungsgemeinschaft and by the Office of Basic Energy Sciences, Division of Chemical Sciences of the U. S. Department of Energy under contract DE-AC03-76SF00098.

10 May 2007; accepted 18 September 2007
10.1126/science.1144959


# Accelerated Uplift and Magmatic Intrusion of the Yellowstone Caldera, 2004 to 2006


**Wu-Lung Chang,[1]* Robert B. Smith,[1]* Charles Wicks,[2] Jamie M. Farrell,[1] Christine M. Puskas[1]**



The Yellowstone caldera began a rapid episode of ground uplift in mid-2004, revealed by Global Positioning System and interferometric synthetic aperture radar measurements, at rates up to 7 centimeters per year, which is over three times faster than previously observed inflation rates. Source modeling of the deformation data suggests an expanding volcanic sill of ~1200 square kilometers at a 10-kilometer depth beneath the caldera, coincident with the top of a seismically imaged crustal magma chamber. The modeled rate of source volume increase is 0.1 cubic kilometer per year, similar to the amount of magma intrusion required to supply the observed high heat flow of the caldera. This evidence suggests magma recharge as the main mechanism for the accelerated uplift, although pressurization of magmatic fluids cannot be ruled out.


The Yellowstone volcanic field is the largest in North America (Fig. 1A). The youngest of three giant eruptions that formed the field occurred 640,000 years ago, creating the 40-km-wide by 60-km-long Yellowstone caldera. This eruption was followed by 30 smaller eruptions of dominantly rhyolite flows, the youngest 70,000 years ago (*1*). Earthquakes, ground deformation, very high heat flow, and the world's largest distribution of hydrothermal features characterize Yellowstone (*2*, *3*), similar to those of other silicic volcanic fields such as Long Valley, California, and Phlegrean Fields, Italy (*4*, *5*).

Geodetic measurements of Yellowstone from 1923 to 2004 using precise leveling, GPS (Global Positioning System), and InSAR (interferometric synthetic aperture radar) have revealed multiple episodes of caldera uplift and subsidence, with maximum average rates of ~1 to 2 cm/year generally centered at its two resurgent domes, Sour Creek and Mallard Lake (*6*–*8*). In addition, an area northwest of the caldera near Norris Geyser Basin experienced periods of substantial ground deformation (*8*, *9*). These spatial and temporal variations of the Yellowstone unrest also correlated with pronounced changes in seismic and hydrothermal activity (*9*, *10*) (Fig. 1B).


[1]Department of Geology and Geophysics, University of Utah, Salt Lake City, UT 84112, USA. [2]U.S. Geological Survey, MS 977, Menlo Park, CA 94025, USA.

*To whom correspondence should be addressed. E-mail: wchang@earth.utah.edu (W.-L.C.); R.Smith@earth.utah.edu (R.B.S.)